LETTER

doi:10.1038/nature11004

A perovskitic lower mantle inferred from high-pressure, high-temperature sound velocity data

Motohiko Murakami[1], Yasuo Ohishi[2], Naohisa Hirao[2] & Kei Hirose[3,4]

The determination of the chemical composition of Earth's lower mantle is a long-standing challenge in earth science. Accurate knowledge of sound velocities in the lower-mantle minerals under relevant high-pressure, high-temperature conditions is essential in constraining the mineralogy and chemical composition using seismological observations[1], but previous acoustic measurements were limited to a range of low pressures and temperatures. Here we determine the shear-wave velocities for silicate perovskite and ferropericlase under the pressure and temperature conditions of the deep lower mantle using Brillouin scattering spectroscopy[2]. The mineralogical model that provides the best fit to a global seismic velocity profile[1] indicates that perovskite constitutes more than 93 per cent by volume of the lower mantle, which is a much higher proportion than that predicted by the conventional peridotitic mantle model. It suggests that the lower mantle is enriched in silicon relative to the upper mantle, which is consistent with the chondritic Earth model. Such chemical stratification implies layered-mantle convection with limited mass transport between the upper and the lower mantle.

It is widely accepted, on the basis of petrological evidence, that at least Earth's uppermost mantle, perhaps down to the top of the mantle transition zone, has a peridotitic (pyrolitic) bulk composition[3,4]. However, a variety of chemical compositions, ranging from peridotitic to chondritic, have been proposed for the lower mantle. The correct composition has long remained a matter of debate owing to a lack of conclusive arguments. Because the isochemical phase transitions in $(Mg,Fe)_2SiO_4$ well explain the global existence of the seismic discontinuities at depths of ~410 and ~660 km (ref. 5), the lower mantle has been conventionally been considered to be peridotitic in composition, with a Mg/Si ratio of ~1.3. The same ratio is found in the upper mantle, which is dominated by $(Mg,Fe)_2SiO_4$ olivine. However, this Mg/Si ratio is significantly higher than that of chondritic meteorites (Mg/Si $\approx$ 1.0), which are usually assumed to be similar in composition to the materials from which Earth formed. The apparent depletion of silicon in the mantle (the 'missing silicon' problem) has provoked much debate that the shortfall is balanced by the presence of silicon in the core[6] or relative silicon enrichment in the lower mantle. Such chemical stratification in the mantle should have occurred during the solidification of the massive magma ocean at the very beginning of Earth's history[7]. Subsequent solid-state convection tends to homogenize the mantle, but the primordial chemical stratification may still be preserved today. This issue is strongly related to the sort of convection that took place in the mantle throughout Earth's history. It has also been proposed that Earth formed preferentially from meteorites with higher Mg/Si ratios owing to the possible radial chemical zonation in the Solar System[8].

The mineral assemblage of the lower mantle has been examined using density measurements under high-pressure (P), high-temperature (T) conditions[9,10]. However, recent computer simulations demonstrated that such experimentally derived density and bulk modulus do not place unique constraints on mantle composition, owing to their intrinsic uncertainties, whereas data on shear velocity (V_S) strongly constrain the lower-mantle models[11]. It is thus crucial to obtain the reliable V_S data on the major lower-mantle constituents, namely silicate perovskite (pv) and (Mg,Fe)O ferropericlase (fp), under relevant high-pressure, high-temperature conditions. Recent progress in Brillouin scattering spectroscopy optimized for extreme high-pressure conditions has enabled us to measure V_S for $MgSiO_3$ pv[12], post-pv[13], and MgO periclase[14] at pressures up to 172 GPa. Although those sound velocity data do provide valuable information on the lower-mantle mineralogy, the effects of chemical impurity and high temperature remain unsettled. Although aluminium impurity was reported to have a strong effect on thermoelastic properties of pv[15], the sound velocity of aluminium-bearing $MgSiO_3$ pv has been measured only below 45 GPa (refs 16, 17). The crossover from high-spin iron to low-spin iron in fp[18] may have an anomalous effect on elasticity at pressures found in the mid-lower mantle[19], but available sound velocity data for fp, especially for its low-spin state, are still limited. More importantly, sound velocity measurements for pv and fp have never been performed under simultaneous high-pressure and high-temperature conditions corresponding to those in the lower mantle. In this work, we determined V_S for aluminous silicate pv (Al pv) and fp at pressures up to 124 GPa and at $T = 300$ K. The high-pressure, high-temperature measurements were also conducted on $MgSiO_3$ pv and MgO at $T = 2{,}700$ K and at pressures up to 91 GPa by using a new Brillouin scattering system[2].

We obtained very sharp Brillouin peaks from the transverse acoustic modes of each phase over the entire P–T range we explored (Fig. 1 and Supplementary Tables 1–4). No significant peak broadening was observed with increasing pressure. The results demonstrate slightly lower values of V_S for $MgSiO_3$(+4 wt% Al_2O_3) pv than for pure $MgSiO_3$ pv[12] at equivalent pressures (Fig. 2a). An anomalous velocity change was observed for $(Mg_{0.92}Fe_{0.08})O$ fp at around 40–60 GPa (Fig. 2b), which is attributed to the iron spin crossover. A flattening of the velocity up to 50 GPa and then its steep increase to 60 GPa are in excellent agreement with recent Brillouin scattering measurements[20]. However, we did not find evidence for elastic softening at the spin crossover as previously reported on the basis of impulsive stimulated scattering spectroscopy[19]. At pressures greater than 60 GPa, V_S increased slowly with pressure relative to its behaviour for pure MgO.

These P–V_S profiles of Al pv and fp were fitted to the third-order Eulerian finite-strain equation[21] to obtain the adiabatic shear modulus (G_0) and its pressure derivative ($G_0' = dG/dP$). For this regression, the zero-pressure volume and the isothermal bulk modulus and its pressure derivative were adopted from recent experiments[9,17]. We obtained best-fit values of $G_0 = 166(1)$ GPa and $G_0' = 1.57(5)$ for Al pv. This G_0 value is consistent with the previous result of 165(2) GPa determined under ambient conditions[16]. The G_0' value is consistent with the value of 1.56(4) obtained for pure $MgSiO_3$ pv[12], indicating the minimal effect of aluminium on G_0'. For fp, the finite-strain fits were made separately

[1]Department of Earth and Planetary Materials Science, Graduate School of Science, Tohoku University, Sendai, Miyagi 980-8578, Japan. [2]Japan Synchrotron Radiation Research Institute, Sayo, Hyogo 679-5198, Japan. [3]Department of Earth and Planetary Sciences, Tokyo Institute of Technology, Meguro, Tokyo 152-8551, Japan. [4]Institute for Research on Earth Evolution, Japan Agency for Marine-Earth Science and Technology, Yokosuka, Kanagawa 237-0061, Japan.

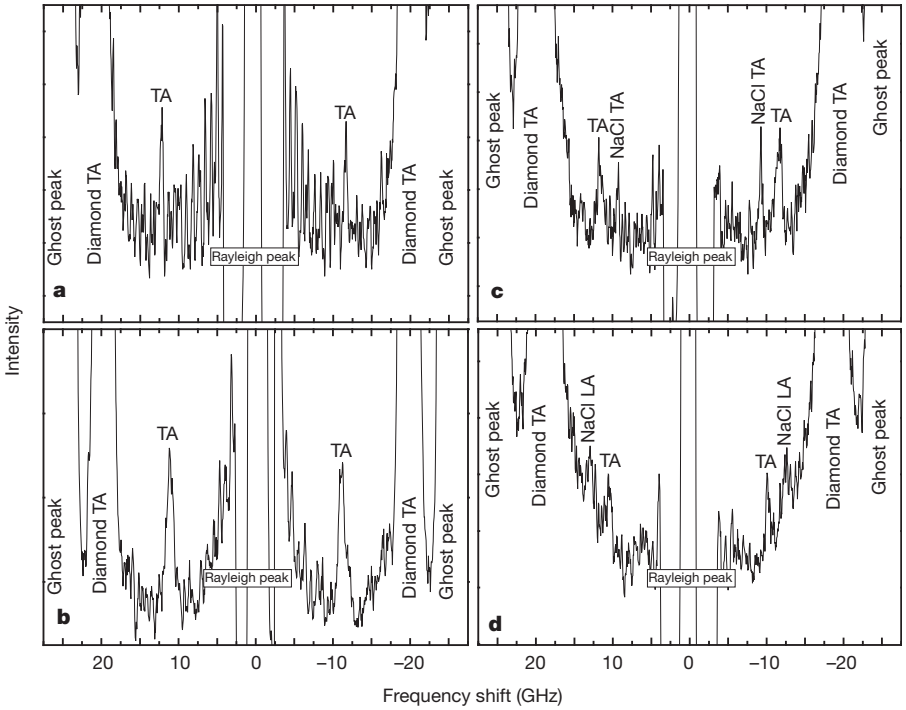

Figure 1 | Brillouin spectra of lower-mantle phases. **a**, $MgSiO_3$(+4 wt% Al_2O_3) pv at 95 GPa and 300 K; **b**, $(Mg_{0.92}Fe_{0.08})O$ at 86 GPa and 300 K; **c**, $MgSiO_3$ pv at 91 GPa and 2,700 K; and **d**, MgO at 48 GPa and 2,700 K. TA and LA indicate transverse and longitudinal acoustic modes of the Brillouin shift, respectively. Ghost peaks are artefacts of the interferometry method used.

for low-pressure (5–40 GPa) and high-pressure (60–121 GPa) because anomalous behaviour was observed at around 50 GPa as a result of spin crossover. The fitting result gives $G_0 = 113(2)$ GPa and $G_0' = 2.15(5)$ for the high-spin state, and $G_0 = 130(2)$ GPa and $G_0' = 2.04(5)$ for the low-spin state. Extrapolation of the high-spin data to high pressure does not reproduce the low-spin data, supporting the proposal that the spin crossover of iron is not associated with elastic softening[19].

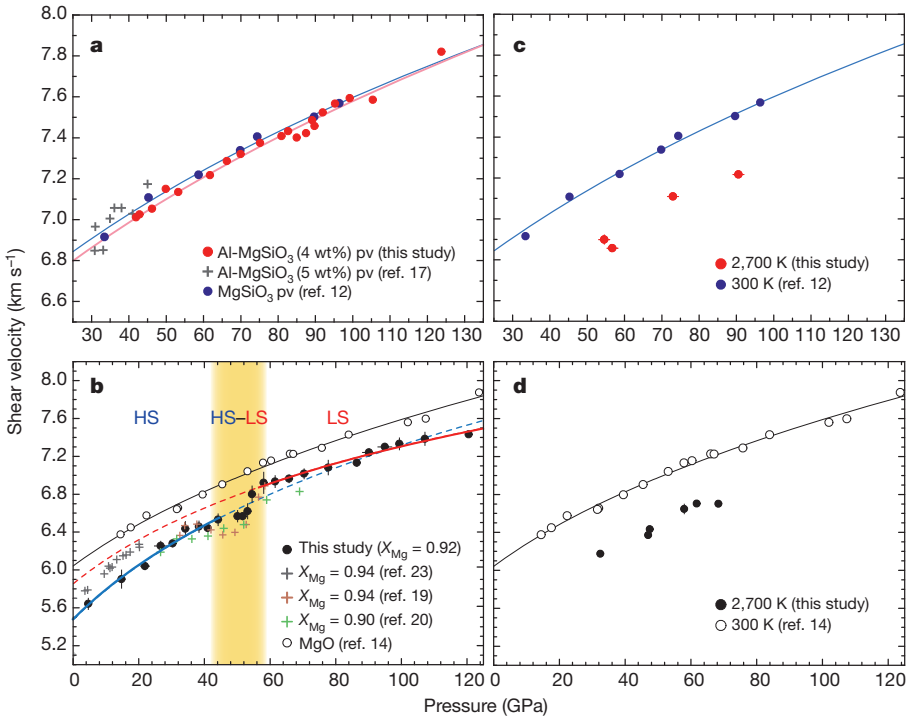

Figure 2 | Shear velocity for lower-mantle phases. **a**, $MgSiO_3$(+4 wt% Al_2O_3) pv at 300 K. Previous data on $MgSiO_3$(+5 wt% Al_2O_3) pv[17] and pure $MgSiO_3$ pv[12] are also shown. Lines show the regression lines obtained from finite-strain fits. **b**, $(Mg_{0.92}Fe_{0.08})O$ fp and previous data on fp[19,20,23] and MgO[14] at 300 K. The shaded zone indicates the pressure range of the iron spin crossover. Blue and red lines respectively show the regression lines obtained from finite-strain fit of $(Mg_{0.92}Fe_{0.08})O$ for high-spin (HS) and low-spin (LS) states of iron. **c**, $MgSiO_3$ pv at 300 K (ref. 12) and 2,700 K. **d**, MgO at 300 K (ref. 14) and 2,700 K. We note that our data on $(Mg_{0.92}Fe_{0.08})O$ yield a lower velocity than do those on $(Mg_{0.94}Fe_{0.06})O$ (ref. 23) owing to higher density. Errors, 1σ.

These G_0 and G_0' values for Al pv and fp are plotted together with previous data[12,17,22–25] in Fig. 3 as a function of iron or aluminium content. Using such relationships, we can estimate G_0 and G_0' for the representative mantle composition ($X_{Mg} = 79$ mol% for fp and $X_{Al_2O_3} = 4$ wt% for pv). The high-pressure, high-temperature measurements on pure $MgSiO_3$ pv and MgO showed that on average the velocity decreased by ~4% and ~6%, respectively, in those compounds at 2,700 K, relative to the values at room temperature[12,14] and at pressures corresponding to the lower mantle (Fig. 2c, d). A linear fit of the shear moduli as functions of pressure, combined with the reported values of G_0 and G_0' (refs 12, 14), provides temperature derivatives of the shear modulus: we find that $dG/dT = -0.020(1)$ GPa K^{-1} for both pv and MgO. The shear strain derivatives of the Grüneisen parameter (γ) are estimated to be $\eta_{S0} = 2.4(2)$ for pv and 3.0(3) for MgO (Supplementary Table 5).

Present measurements performed over a wide P–T range that covers almost all lower-mantle conditions allow us to constrain the lower-mantle mineralogy[12,14]. We model the lower mantle as a two-phase mixture of pv and fp in a SiO_2-MgO-FeO-Al_2O_3 system in which (Al,Fe)-bearing pv contains 4 wt% Al_2O_3 with $X_{Mg} = 94$ mol% and fp has $X_{Mg} = 79$ mol% (ref. 26). A constant Mg-Fe partitioning coefficient between pv and fp is assumed for the entire lower mantle. The V_S profiles of pv and fp with the stated compositions were calculated along the typical temperature profiles. Among several different lower-mantle geotherms, here we consider two extreme cases, one for whole-mantle convection[27] and one for layered-mantle convection[28] (Fig. 4a). We did our calculations using the recent compilation of elastic parameters given in the formalism in ref. 21 and using the thermoelastic parameters determined here (Fig. 3 and Supplementary Table 5). The trade-offs between Mg/Fe or Mg/Si and thermal parameters were discussed in previous studies[11,21]. The aggregate V_S value of the two-phase assemblage was obtained by the Voigt–Reuss–Hill averaging method.

We compared the calculated V_S profiles with the Preliminary Reference Earth Model[1] (PREM), a one-dimensional global seismic model. For the whole-mantle convection geotherm, the PREM is best fitted by the mixture of 95% pv and 5% fp by volume ($X_{pv} = 0.95$; Fig. 4b). The goodness-of-fit for this regression ($R^2 = 0.996$) indicates an excellent agreement with the PREM model. The velocity for fp increases steeply by ~4% across the spin crossover (Fig. 2b); however, such an anomalous feature is not clear in the calculated profile of the pv + fp mixture, suggesting that the spin crossover of iron in fp may be seismologically unrecognizable. By contrast, the V_S profile for a peridotitic (pyrolitic) mantle[26] ($X_{pv} = 0.80$) is lower than the PREM by up to 3.2% throughout the pressure range of the lower mantle, indicating that the conventional peridotitic model is incompatible with the seismological observations.

Such regression suggests that the mantle is not chemically homogeneous and hence implies layered-mantle convection. We therefore applied the layered-mantle convection geotherm and found that the PREM profile is reproduced only by pv without any fp ($R^2 = 0.995$; Fig. 4c), providing further evidence that the mantle is not peridotitic. To verify the internal consistency of those regression results, we also calculated the longitudinal velocity ($V_P = \sqrt{(K + 4G/3)/\rho}$) profile using the bulk modulus (K) and density (ρ) determined from recent X-ray diffraction data[9,10] (G, shear modulus). The results show that $X_{pv} = 0.93$ ($R^2 = 0.999$; Fig. 4d), consistent with the value estimated from the V_S profile. $CaSiO_3$ perovskite (cpv) is also believed to be present in the lower mantle as a host of calcium. There are no experimental data on the sound velocity for cpv under the pressure conditions in the lower mantle, and theoretical predictions are still controversial[29,30]. Nevertheless, cpv is a volumetrically minor (~5%) phase in the lower mantle and the incorporation of cpv thus does not change the present modelling results appreciably.

The main uncertainties in our mineralogical modelling reflect the errors in the thermodynamic and thermoelastic parameters we have used. The effect of temperature on shear modulus is most sensitive to η_{S0} (ref. 21), which was determined for both pv and MgO with an uncertainty of ±10% in our high-pressure, high-temperature measurements. Also, the Mg-Fe partitioning between pv and fp (quantified by the coefficient K_D) remains controversial. Nevertheless, we found that the fitting results for X_{pv} are fairly insensitive to these η_{S0} and K_D values in modelling reported here. Indeed, the 10% uncertainties in η_{S0}

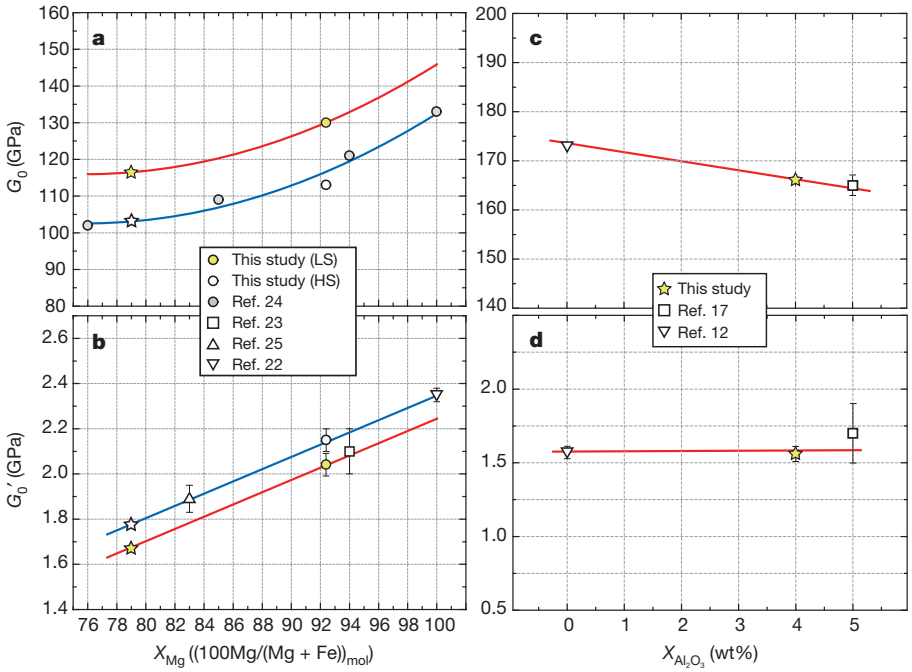

Figure 3 | Effect of aluminium and iron on shear modulus and its pressure derivative. **a**, **b**, (Mg,Fe)O fp; and **c**, **d**, aluminum-bearing $MgSiO_3$ pv. Stars represent G_0 (**a**, **c**) or G_0' (**b**, **d**) for representative iron and Al_2O_3 contents of $X_{Mg} = 79$ mol% (ref. 26) for fp and $X_{Al_2O_3} = 4$ wt% for pv. Lines show the best-fit trends. Blue and red lines in **a** and **b** indicate the trends of (Mg,Fe)O for the high-spin and low-spin states of iron, respectively. The nonlinear relationship between G_0 and iron content in **a** is based on the results of ref. 24. Errors, 1σ.

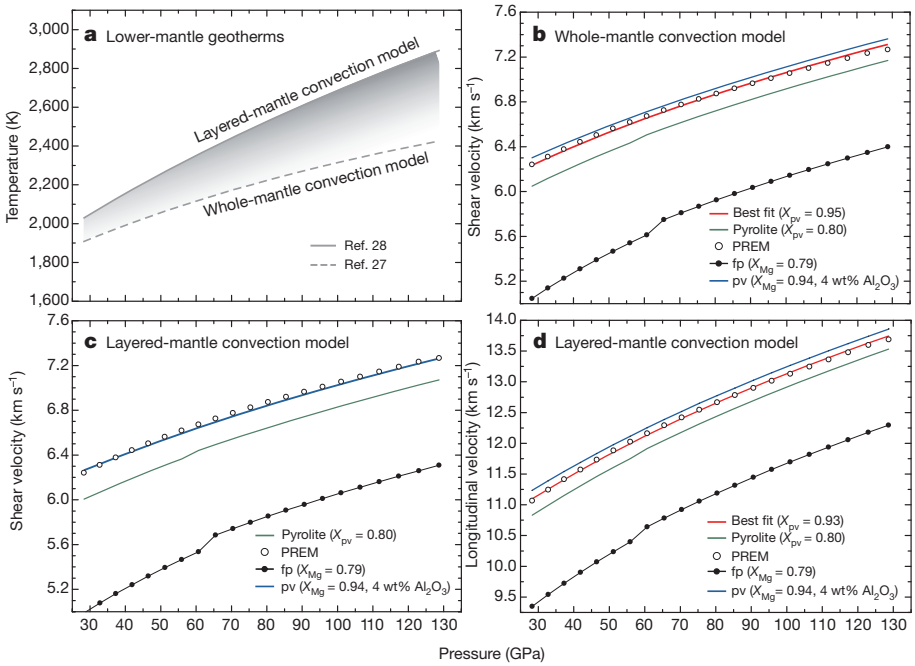

Figure 4 | Lower-mantle geotherms and calculated shear- and longitudinal-wave velocity profiles for whole-mantle and layered-mantle convection models. **a**, Representative lower-mantle geotherms for whole-mantle convection[27] and layered-mantle convection[28] models. **b**–**d**, Calculated shear- (**b**, **c**) and longitudinal-wave (**d**) velocity profiles of fp (black lines) and pv (blue lines) for whole-mantle and layered-mantle convection. The velocity profile for the pyrolitic model is presented as a green line. The best-fit models to the PREM are shown as red curves, indicating the pv-dominant (>93 vol%) lower mantle.

and in K_D change X_{pv} by less than 2% and 0.35%, respectively. In addition, the 30% variation in the G_0' value for fp, which is consistent with almost all previously reported data and corresponds to the uncertainty in the determination here (Fig. 3b), changes X_{pv} by only ~2%, which is small enough still to support our perovskitic lower-mantle model.

Our results indicate that the conventional peridotitic mantle model is not compatible with the seismic properties of the lower mantle, even considering the experimental uncertainties, and strongly suggest that the lower mantle is dominated by perovskite (>93 vol%) and is therefore silica-rich by comparison with the upper mantle. The lower mantle is chemically distinct, with a near-chondritic Mg/Si ratio (~1.0), which reasonably explains the 'missing silicon' problem. The difference in chemical composition between the upper and the lower mantle could be a consequence of fractional crystallization of the magma ocean extending to the deep lower mantle[7] in the early history of Earth. The primordial chemical stratification could be preserved through the subsequent solid-state convection until the present day. Previous mantle convection simulations have demonstrated that a flow pattern evolves from layered- to whole-mantle convection owing to a decrease in the Rayleigh number with cooling[31]. For this reason, layered-mantle convection is presumed to be predominant in the early Earth, indicating that mass transport between the upper and the lower mantle was limited. The seismic tomography images of subducting slabs or upwelling plumes penetrating the boundary between the upper and the lower mantle[32] may not represent whole-mantle convection but rather an intermittent or transitional stage between layered- and whole-mantle convection.

The boundary between the upper and the lower mantle may be of chemical origin. Recent density measurements under relevant P–T conditions of the lower mantle[10] and computational simulations[11] both also suggest that physical properties of the lower mantle are difficult to reconcile with the peridotitic mantle model but are more consistent with the perovskite-rich lower-mantle models. The lack of internal consistency of the conventionally used pressure scales in the previous high-pressure experiments also requires reconsideration of the interpretation of the 660-km seismic discontinuity. Detailed reassessment of the post-spinel phase-transition boundary on the basis of a newly established pressure scale has indeed demonstrated that the depth of the 660-km seismic discontinuity does not match the pressure of this phase transition[33], indicating the incompatibility with an isochemical peridotitic mantle model. The density contrast at the boundary between the peridotitic and the near-chondritic mantle is found to be high enough to allow layered-mantle convection[31]. A dense, stiff, pv-rich lower mantle would promote separate convection and thus inhibit chemical homogenization.

METHODS SUMMARY

We determined the sound velocities of lower-mantle minerals by using a newly developed system at beamline BL10XU of SPring-8 (ref. 2). The shear-wave velocity data were collected, with reference to the Brillouin scattering measurements, at high pressure in a diamond-anvil cell. A carbon dioxide laser was used to heat the sample, and the sample temperature was determined and monitored by a spectroradiometric method in high-temperature experiments. Synchrotron X-ray diffraction measurements were simultaneously performed to determine the lattice parameters (volume) of the sample and the pressure standard.

Full Methods and any associated references are available in the online version of the paper at www.nature.com/nature.

Received 5 July 2011; accepted 28 February 2012.

1. Dziewonski, A. M. & Anderson, D. L. Preliminary reference Earth model. *Phys. Earth Planet. Inter.* **25,** 297–356 (1981).
2. Murakami, M. *et al.* Development of in-situ Brillouin spectroscopy at high pressure and temperature with synchrotron radiation and infrared laser heating system: application to the Earth's deep interior. *Phys. Earth Planet. Inter.* **174,** 282–291 (2009).
3. Ringwood, A. E. *Composition and Petrology of the Earth's Mantle* (McGraw Hill, 1975).
4. Sun, S. S. Chemical-composition and origin of the Earth's primitive mantle. *Geochim. Cosmochim. Acta* **46,** 179–192 (1982).
5. Ito, E. & Takahashi, E. Postspinel transformations in the system Mg_2SiO_4-Fe_2SiO_4 and some geophysical implications. *J. Geophys. Res.* **94,** 10637–10646 (1989).
6. Allègre, C. J., Poirier, J. P., Humler, E. & Hofmann, A. W. The chemical composition of the earth. *Earth Planet. Sci. Lett.* **134,** 515–526 (1995).
7. Tonks, W. B. & Melosh, H. J. Magma ocean formation due to giant impact. *J. Geophys. Res.* **98,** 5319–5333 (1993).
8. Ringwood, A. E. Significance of the terrestrial Mg/Si ratio. *Earth Planet. Sci. Lett.* **95,** 1–7 (1989).

9. Fei, Y. *et al.* Spin transition and equations of state of (Mg, Fe)O solid solutions. *Geophys. Res. Lett.* **34,** L17307 (2007).
10. Ricolleau, A. *et al.* Density profile of pyrolite under the lower mantle conditions. *Geophys. Res. Lett.* **36,** L06302 (2009).
11. Mattern, E., Matas, J., Ricard, Y. & Bass, J. Lower mantle composition and temperature from mineral physics and thermodynamic modelling. *Geophys. J. Int.* **160,** 973–990 (2005).
12. Murakami, M., Sinogeikin, S. V., Hellwig, H., Bass, J. D. & Li, J. Sound velocity of $MgSiO_3$ perovskite to Mbar pressure. *Earth Planet. Sci. Lett.* **256,** 47–54 (2007).
13. Murakami, M. *et al.* Sound velocity of $MgSiO_3$ post-perovskite phase: a constraint on the D'' discontinuity. *Earth Planet. Sci. Lett.* **259,** 18–23 (2007).
14. Murakami, M., Ohishi, Y., Hirao, N. & Hirose, K. Elasticity of MgO to 130GPa: implications for lower mantle mineralogy. *Earth Planet. Sci. Lett.* **277,** 123–129 (2009).
15. Brodholt, J. P. Pressure-induced changes in the compression mechanism of aluminous perovskite in the Earth's mantle. *Nature* **407,** 620–622 (2000).
16. Jackson, J. M., Zhang, J. & Bass, J. D. Sound velocities and elasticity of aluminous $MgSiO_3$ perovskite: implications for aluminum heterogeneity in Earth's lower mantle. *Geophys. Res. Lett.* **31,** L10614 (2004).
17. Jackson, J. M., Zhang, J., Shu, J., Sinogeikin, S. V. & Bass, J. D. High-pressure sound velocities and elasticity of aluminous $MgSiO_3$ perovskite to 45 GPa: implications for lateral heterogeneity in Earth's lower mantle. *Geophys. Res. Lett.* **32,** L21305 (2005).
18. Badro, J. *et al.* Iron partitioning in Earth's mantle: toward a deep lower mantle discontinuity. *Science* **300,** 789–791 (2003).
19. Crowhurst, J. C., Brown, J. M., Goncharov, A. F. & Jacobsen, S. D. Elasticity of (Mg,Fe)O through the spin transition of iron in the lower mantle. *Science* **319,** 451–453 (2008).
20. Marquardt, H., Speziale, S., Reichmann, H. J., Frost, D. J. & Schilling, F. R. Single-crystal elasticity of $(Mg_{0.9}Fe_{0.1})O$ to 81 GPa. *Earth Planet. Sci. Lett.* **287,** 345–352 (2009).
21. Stixrude, L. & Lithgow-Bertelloni, C. Thermodynamics of mantle minerals - I. Physical properties. *Geophys. J. Int.* **162,** 610–632 (2005).
22. Kennett, B. L. N. & Jackson, I. Optimal equations of state for mantle minerals from simultaneous non-linear inversion of multiple datasets. *Phys. Earth Planet. Inter.* **176,** 98–108 (2009).
23. Jackson, J. M. *et al.* Single-crystal elasticity and sound velocities of $(Mg_{0.94}Fe_{0.06})O$ ferropericlase to 20 GPa. *J. Geophys. Res.* **111,** B09203 (2006).
24. Jacobsen, S. D. *et al.* Structure and elasticity of single-crystal (Mg,Fe)O and a new method of generating shear waves for gigahertz ultrasonic interferometry. *J. Geophys. Res.* **107,** 2037 (2002).
25. Kung, J., Li, B. S., Weidner, D. J., Zhang, J. Z. & Liebermann, R. C. Elasticity of $(Mg_{0.83},Fe_{0.17})O$ ferropericlase at high pressure: ultrasonic measurements in conjunction with X-radiation techniques. *Earth Planet. Sci. Lett.* **203,** 557–566 (2002).
26. Jackson, I. & Rigden, S. M. in *The Earth's Mantle: Composition, Structure and Evolution* (ed. Jackson, I.) 405–460 (Cambridge Univ. Press, 1998).
27. Brown, J. M. & Shankland, T. J. Thermodynamic parameters in the Earth as determined from seismic profiles. *Geophys. J. R. Astron. Soc.* **66,** 579–596 (1981).
28. Anderson, O. L. The Earth's core and the phase-diagram of iron. *Phil. Trans. R. Soc. Lond. A* **306,** 21–35 (1982).
29. Li, L. *et al.* Elasticity of $CaSiO_3$ perovskite at high pressure and high temperature. *Earth Planet. Sci. Lett.* **155,** 249–259 (2006).
30. Stixrude, L., Lithgow-Bertelloni, C., Kiefer, B. & Fumagalli, P. Phase stability and softening in $CaSiO_3$ perovskite at high pressure. *Phys. Rev. B* **75,** 024108 (2007).
31. Christensen, U. R. & Yuen, D. A. Layered convection induced by phase-transitions. *J. Geophys. Res.* **90,** 10291–10300 (1985).
32. van der Hist, R., Engdahl, R., Spakman, W. & Nolet, G. Tomographic imaging of subducted lithosphere below northwest Pacific island arcs. *Nature* **353,** 37–43 (1991).
33. Tange, Y., Nishihara, Y. & Tsuchiya, T. Unified analyses for P-V-T equation of state of MgO: a solution for pressure-scale problems in high P-T experiments. *J. Geophys. Res.* **115,** B12203 (2010).

Supplementary Information is linked to the online version of the paper at www.nature.com/nature.

Acknowledgements We greatly appreciate the comments by I. Jackson. Suggestions from E. Ohtani, C. Bina, S. Karato and S.-H. Shim improved the manuscript. We also thank N. Sata and Y. Asahara for their experimental assistance at SPring-8. This study was performed under the approval of SPring-8 (proposals no. 2008B0099 and 2009A0087).

Author Contributions M.M. planned the research and did experimental and analytical work. M.M. and K.H. wrote the paper. All authors were involved in the experiments and discussed the results.

Author Information Reprints and permissions information is available at www.nature.com/reprints. The authors declare no competing financial interests. Readers are welcome to comment on the online version of this article at www.nature.com/nature. Correspondence and requests for materials should be addressed to M.M. (motohiko@m.tohoku.ac.jp).

METHODS

Starting materials. Gel starting materials were used for experiments on both $MgSiO_3$ and aluminous $MgSiO_3$ pv. The $MgSiO_3$ gel was the same as that used in previous high-pressure experiments on post-pv[34]. The chemical composition of aluminous $MgSiO_3$ gel is shown in Supplementary Table 6. For the experiments on MgO, fine-grained (~1 μm in diameter) polycrystalline powder was used[14]. The $(Mg_{0.92}Fe_{0.08})O$ fp sample was synthesized by mixing stoichiometric amounts of MgO and Fe_2O_3 powder, heating the mixture overnight at 1,200 °C in reducing conditions using a H_2/CO_2 gas-flow furnace, and then quenching. The X-ray diffraction measurement for well-ground fine powder showed a lattice constant of $a = 4.2209(5)$ Å, indicating that the iron content in this fp sample is $(Mg_{0.924}Fe_{0.076})O$ (ref. 24), in excellent agreement with the target composition ($(Mg_{0.92}Fe_{0.08})O$).

Brillouin scattering measurements. High-pressure, high-temperature Brillouin scattering measurements of sound velocities were carried out in a laser-heated diamond-anvil cell with a 60° angular aperture. A diode-pumped laser with a wavelength of 532 nm was used as a probe beam. An incident laser was focused to a beam size of diameter ~20 μm on the sample. The scattered light was analysed using a six-pass tandem Fabry–Pérot interferometer. All the measurements were performed in a platelet scattering geometry. The scattering angle was calibrated using the glass standard material BK7 in each run. A pre-pressed plate of polycrystalline/gel sample with a thickness of about 30 μm was loaded into a hole (100 μm in diameter) drilled in a rhenium gasket sandwiched between NaCl plates that served as a pressure medium and a thermal insulator.

Polycrystalline pv samples were synthesized *in situ* in a diamond-anvil cell from the gel starting materials by heating with a CO_2 laser. Pressure was determined on the basis of the Raman T_{2g} mode of the diamond anvil[35] or the equations of state of NaCl[36] at ambient temperature and Pt[37] and MgO[38] at high temperature. At each pressure, the raw Brillouin spectra of Stokes and anti-Stokes peaks were fitted with a Gaussian peak function to determine the peak positions. We obtained Brillouin spectra on compressed samples in nine, six, three and four separate runs for aluminous $MgSiO_3$ pv, fp, $MgSiO_3$ pv and MgO, respectively. Each Brillouin spectrum was collected in 2–16 h.

The angle dispersive X-ray diffraction measurements were conducted simultaneously to determine the volume of the sample and the pressure at BL10XU, the synchrotron X-ray source at SPring-8 in the energy range 30–40 keV (Supplementary Fig. 1). The sample temperature was determined and monitored by a spectroradiometric method in the high-temperature experiments. The heating spot of the CO_2 laser was typically 40–50 μm in diameter (Supplementary Fig. 2), which was sufficiently larger than the beam spot for the Brillouin measurements. The temporal fluctuation in temperature during heating did not exceed 200 K. As shown in Supplementary Fig. 1, the X-ray diffraction peaks for each sample were very sharp. The two-dimensional X-ray diffraction images showed clear circular Debye rings with a fairly uniform intensity distribution along the circle, indicating that there was no significant grain growth or lattice preferred orientation in the sample at high pressure and high temperature.

Ambient volume of fp in the low-spin state. To obtain the zero-pressure shear modulus and its pressure derivative for the fp sample in the low-spin state, we need to determine the volume under ambient conditions (V_0). Assuming a linear relationship between V_0 and iron content in low-spin fp as reported in ref. 9, for our sample we estimate that $V_0 = 74.59$ Å^3.

34. Murakami, M., Hirose, K., Kawamura, K., Sata, N. & Ohishi, Y. Post-perovskite phase transition in $MgSiO_3$. *Science* **304,** 855–858 (2004).
35. Akahama, Y. & Kawamura, H. High-pressure Raman spectroscopy of diamond anvils to 250 GPa: method for pressure determination in the multimegabar pressure range. *J. Appl. Phys.* **96,** 3748–3751 (2004).
36. Sata, N., Shen, G., Rivers, M. L. & Sutton, S. R. Pressure-volume equation of state of the high-pressure B2 phase of NaCl. *Phys. Rev. B* **65,** 104114 (2002).
37. Holmes, N. C., Moriarty, J. A., Gathers, G. R. & Nellis, W. J. The equation of state of platinum to 660 GPa (6.6Mbar). *J. Appl. Phys.* **66,** 2962–2967 (1989).
38. Dewaele, A., Fiquet, G., Andrault, D. & Hausermann, D. P-V-T equation of state of periclase from synchrotron radiation measurements. *J. Geophys. Res.* **105,** 2869–2877 (2000).